APPLIED PHYSICS

Remote detection of radioactive material using mid-IR laser–driven electron avalanche

Robert M. Schwartz, Daniel Woodbury, Joshua Isaacs, Phillip Sprangle, Howard M. Milchberg*

Remote detection of a distant, shielded sample of radioactive material is an important goal, but it is made difficult by the finite spatial range of the decay products. Here, we present a proof-of-principle demonstration of a remote detection scheme using mid-infrared (mid-IR) ($\lambda = 3.9\ \mu m$) laser–induced avalanche breakdown of air. In the scheme's most basic version, we observe on-off breakdown sensitivity to the presence of an external radioactive source. In another realization of the technique, we correlate the shift of the temporal onset of avalanche to the degree of seed ionization from the source. We present scaling of the interaction with laser intensity, verify observed trends with numerical simulations, and discuss the use of mid-IR laser–driven electron avalanche breakdown to detect radioactive material at range.

INTRODUCTION

Detecting radioactive material at range remains a difficult technical challenge. Conventional methods such as Geiger counters directly detect radioactive emission whose flux falls off, at best, as the inverse square of the distance from the source, with additional reduction by shielding materials and from absorption in air. In the immediate vicinity of radioactive material, however, high-energy α-, β-, and γ-particles ionize neutral air constituents, elevating the number of free electrons and ions present in the ambient air, providing a source of species for extensive positive and negative ion chemistry. Electron avalanche breakdown seeded by the negative species, and driven at range by a laser source, is one possible method for detecting radioactive material remotely.

In electron avalanche breakdown, intense electromagnetic wave–driven electron collisional heating and ionization initially increases the electron density exponentially, followed by a saturation phase where the growth rate is strongly reduced. Avalanche breakdown was first observed using microwave sources and later with high-power pulsed lasers (*1*–*4*). In the latter case, free electrons in the focal volume (whose origins in this experiment are discussed later) experience driven oscillations in the laser electromagnetic field. These coherently driven electrons undergo weak elastic collisions with atoms and ions, which introduce small phase shifts and direction changes to their orbits, suppressing reradiation of the oscillation energy back into the laser beam. Coherent electron motion driven by the beam is thus converted to incoherent motion or heating. This process is commonly called resistive or inverse Bremsstrahlung heating. A simple estimate of the heating rate is $d\varepsilon/dt \sim 2\nu U_p$ (*5*), where ν is the electron-atom elastic collision rate, $U_p \sim 0.93 \times 10^{-13} I\lambda^2$ (eV) is the time-averaged electron oscillatory energy or ponderomotive potential, I (W/cm^2) is the laser intensity, and λ (μm) is the laser wavelength, illustrating the favorable scaling of heating with laser wavelength. Ionization occurs when the highest-energy electrons have energies exceeding the ionization threshold of neutral air constituents; ionization can then proceed by inelastic collisions. When electron heating and ionization are strong enough to overcome losses such as diffusion, recombination, and radiative cooling, the density of free electrons increases in an exponential cascade, with the time required for the density of electrons to double determined by the laser field strength, wavelength, and local air density. Once the local density of the ionizing species, such as neutral air molecules, declines by more than a few percent, growth is no longer exponential, with electron density increasing at a lower rate until saturation at maximum ionization is reached. At this point, either the gas is fully ionized or the electrons are insufficiently heated during the laser pulse to push the ionization level higher.

One approach to using the avalanche process to detect radioactive sources is to use the sensitivity of the air breakdown time to the initial electron population in the laser focal volume. From a diagnostic perspective, we consider "breakdown time" to be the time delay for the laser-driven ionization to grow to some detectable level. As shown in the simulation of Fig. 1B (see Materials and Methods), differences in the local laser intensity experienced by a seed electron in air can manifest as clear differences in breakdown rate. We later discuss how these differences are measurable in terms of an effective breakdown time.

In previous work, schemes have been proposed to detect shifts in breakdown time in the presence of radioactivity using a high-power terahertz- or millimeter-wave source (*6*, *7*). Recent experiments observed a time shift in air breakdown by a 95-GHz gyrotron in the presence of a 0.64-mCi ^{60}Co source (*8*). Scaling these interactions to long range, however, demands very large diameter focusing elements to counteract the rapid beam diffraction at these long wavelengths, necessitating extremely high-power gyrotrons that are not readily available (*7*). In addition, the long pulse durations of these sources (longer than tens of microseconds) (*7*, *8*) make the breakdown susceptible to random seeding by cosmic rays or diffusion of free electrons or dust particles into the focal volume, complicating the determination of breakdown time.

In addition to free electrons, ion products can also be important for an avalanche-based detection scheme. In particular, the superoxide anion O_2^-, produced by attachment of free electrons to O_2, is the primary ion generated over short time scales after an ionization event (*9*) and is the key precursor species to the subsequent ion sequence in tropospheric negative ion chemistry (*10*–*12*). Because of its low electron detachment energy of 0.45 eV (*13*), O_2^- is a readily accessible source of additional electrons to initiate breakdown. Recent theoretical work on the avalanche detection scheme has suggested using a secondary visible or near-infrared (near-IR) wavelength laser (with a photon energy of >0.45 eV) to first photodetach electrons from O_2^- followed by a pulsed IR laser to drive the electron avalanche (*14*, *15*). Assuming a steady source of ionizing radiation from a radioactive source, a simple rate equation model (see Materials and Methods) (*15*) gives the pre-avalanche ratio of free electron density to O_2^- density, $N_e/N_{O_2^-} \approx 5\beta/\eta N_{O_2} \approx 10^{-6}$, where β is the loss rate of O_2^- due to collisions with

Institute for Research in Electronics and Applied Physics, University of Maryland, College Park, MD 20742, USA.
*Corresponding author. Email: milch@umd.edu

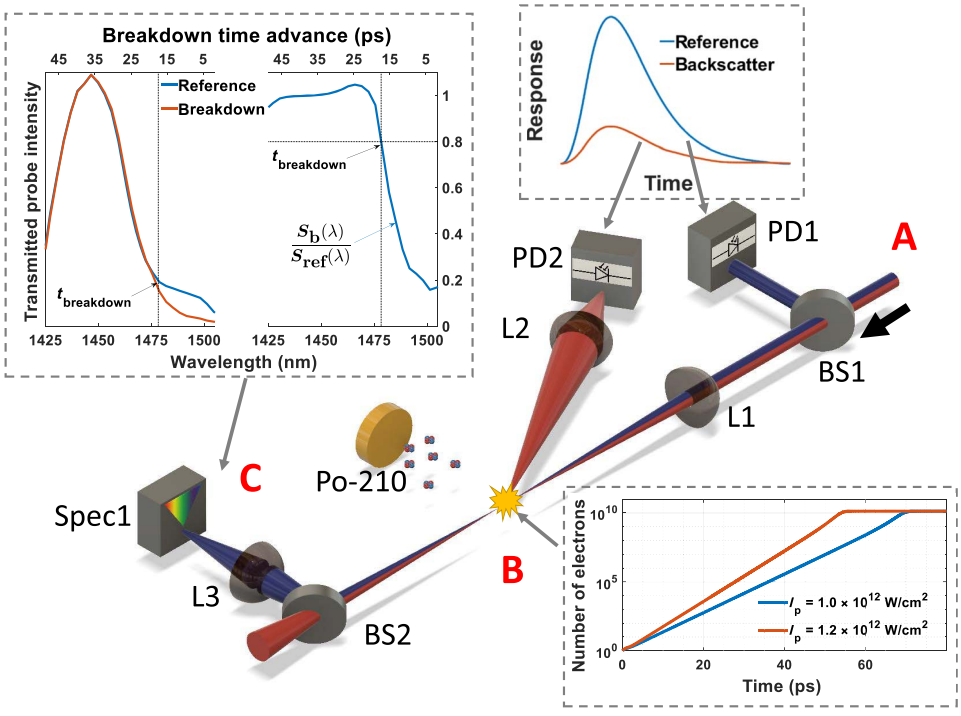

Fig. 1. Radioactive source–seeded mid-IR laser–driven avalanche breakdown of air. (**A**) Copropagating 50-ps (FWHM) λ = 3.9 μm pump and 70-ps (full width) chirped 1.45-μm probe pulses are generated in an OPCPA system (see Materials and Methods for details). Beamsplitter BS1 splits off >99% of the λ = 1.45 μm probe and sends it to PbSe photodetector PD1 for a probe pulse energy reference. This signal is also proportional to the λ = 3.9 μm pump energy (sample trace shown) because of the optical parametric amplification process. (**B**) Ionizing radiation (5.3-MeV α-particles) from an 18-mm-diameter Po-210 foil source generates a population of free electrons and O_2^- ions in the focal region of lens L1, seeding collisional avalanche ionization driven by the λ = 3.9 μm pump. At lower average seed density, a seed electron is less likely to appear in a region of highest laser intensity in the focal volume, and thus, a local breakdown will take longer as shown in the simulation panel. The evolving avalanche breakdown plasma backscatters a portion of the λ = 3.9 μm pump pulse, which is collected by lens L2 onto PbSe photodetector PD2, with a sample trace shown. (**C**) The chirped λ = 1.45 μm probe is transmitted through the plasma, separated from the 3.9-μm pump by beamsplitter BS2 and collected by lens L3 onto InGaAs spectrometer Spec1. The spectral components of the chirped probe pulse correspond to specific time delays, as shown by the shared wavelength and time axis on the inset figure. The rapidly increasing plasma density cuts off the chirped probe at the breakdown time, taken to be the wavelength interval (and corresponding time) where the ratio $S_b(\lambda)/S_{ref}(\lambda)$ is reduced by 20%, where $S_{ref}(\lambda)$ is the probe reference spectrum and $S_b(\lambda)$ is the probe spectrum transmitted through the breakdown region.

neutral air molecules, η is the rate of attachment of electrons to O_2, and N_{O_2} is the density of atmospheric oxygen. Therefore, O_2^- ions are the dominant species for seeding avalanche breakdown.

Here, we report on the proof-of-principle demonstration of mid-infrared (mid-IR) laser–driven avalanche breakdown as a scheme for remote detection of radioactive sources. In the most basic version, we observe on-off sensitivity of the avalanche breakdown of air to the presence of an external radiation source. In another realization of the scheme, we correlate the shift of the breakdown time to the externally supplied initial ionization. The breakdown time is measured by transmission of a chirped probe pulse or backscatter of the pump pulse, detection methods that are robust and relatively insensitive to alignment. Observed shifts in breakdown timing are supported by simulations of the avalanche evolution in the laser field. We discuss scaling of the avalanche breakdown with laser intensity and focal geometry and its extension to standoff geometries of interest to applications in the field.

Our use of a mid-IR wavelength laser (λ = 3.9 μm) at a pulse width of 50 ps to drive avalanches is particularly well suited to radiation detection for multiple reasons: (i) the initial population of free electrons is easily liberated from O_2^- by two-photon ionization without the need for a secondary laser; (ii) the low photon energy at λ = 3.9 μm (~0.25 eV) suppresses the competing effect of higher-order multiphoton ionization (MPI) of neutral species; (iii) for comparable intensities, a long-wavelength laser results in greater plasma heating and stronger avalanche (as discussed earlier); (iv) the pulse duration is long enough to drive an avalanche, allowing clear observation of breakdown time shifts, yet short enough to avoid the complicating effects of air plasma hydrodynamics while the pulse is on; (v) the probability of a dark count in a 50-ps window due to random seeding by cosmic rays, diffusing electrons, or dust is greatly reduced compared with nanosecond pulses; and (vi) compared with nanosecond pulses, reduced energy is needed to drive an avalanche. We note, related to point (ii) above, that with visible or near-IR lasers (Nd:YAG at 1.064 and 0.532 μm, or Ti:sapphire at 0.8 μm), we have observed that the intensity level needed to drive an easily detectable air breakdown also generates many electrons through MPI of neutral air molecules, completely masking the initial population of free electrons induced by the radioactive source (*16*).

The development of an avalanche breakdown requires sufficient plasma heating to overcome losses such as electron attachment, diffusion, and inelastic collisions. For short pulses of duration τ, such as the picosecond pulses in the present experiment, the intensity threshold to reach full collisional breakdown increases as 1/τ to reach full ionization by the end of the pulse. The time-limited air breakdown threshold intensity presented in (*17*) is $I_{th}(W/cm^2) \approx 8 \times 10^2/P\tau\lambda^2$,

where P is pressure (atm), τ is pulse duration (ps) and λ is wavelength (μm). Applying this to our laser parameters (τ = 50 ps, λ = 3.9 μm) in air at 1 atm predicts $I_{th} \approx 1 \times 10^{12}$ W/cm^2. For avalanche breakdown to occur, at least one O_2^- ion must occupy a region close enough to the laser focus that the local intensity is above I_{th}. For a given focal spot size w_0 and peak laser intensity $I_p > I_{th}$, the volume in which breakdown can occur is $V_{br}(w_0, I_p)$ and the number of O_2^- ions within that region is $n_{O_2^-} = V_{br}(w_0, I_p)N_{O_2^-}$. If $n_{O_2^-} \ll 1$, it is highly unlikely that any ions are within this region so no avalanche can occur. For $n_{O_2^-} \sim 1$, a small number of ions are randomly distributed within the laser focus, with a higher probability that they are located in lower-intensity regions. Ions farther from the center of the beam waist will seed a lower avalanche rate. For sufficiently high densities $n_{O_2^-} \gg 1$, there will always be ions close to the highest intensities in the beam focus, seeding the maximum avalanche rate. The fastest breakdown time is thus determined by the peak intensity at the focus, while the statistical average breakdown time is determined by a relationship between seed ion density, laser intensity, and focal geometry.

RESULTS

Avalanche breakdown time shift and pump backscatter

Avalanche breakdown of air was driven by λ = 3.9 μm, 50-ps FWHM (full width at half maximum) mid-IR pulse laser pulses focused at a varying f-number to peak intensities in the range 0.6×10^{12} to 2×10^{12} W/cm^2, with most runs conducted with a laser spot size $w_0 \sim$ 100 μm. The experimental setup is shown in Fig. 1. Avalanche was monitored using transmission of a weak, copropagating chirped probe beam (~10 μJ; λ = 1.4 to 1.5 μm; full width, 70 ps) and backscattering of the λ = 3.9 μm driver pulse. The pump and probe pulses were derived from an ultrafast, mid-IR optical parametric chirped pulse amplifier (OPCPA) laser system (25 mJ; λ = 3.9 μm; compressed pulse width, 90 fs), where the pump and probe beams for the present experiment were not compressed but were left as chirped pulses tens of picoseconds in duration, as described in Materials and Methods.

We note that all radioactive sources of interest, whether α, β, or γ emitters, result in free-electron generation from the ionization of ambient air. In this experiment, we use a 5-mCi Po-210 foil source, which produces 5.3-MeV α-particles. Through collisions with air molecules, the α-particles liberate high-energy electrons, which drive subsequent ionization. The electrons thermalize and then efficiently attach to neutral O_2 within tens of nanoseconds (*15*) to form O_2^-. The avalanche is seeded by two-photon ionization of O_2^- by the temporal leading edge of the mid-IR driver pulse, as will be discussed later. For the Po-210 foil source, the O_2^- concentration is highest within the α-particle stopping distance [continuous slowing down approximation (CSDA)] in air of ~3.5 cm from the source (*18*).

Figure 2 shows the results of the probe transmission and pump backscatter as the Po-210 source is translated toward the pump focal volume. The negatively chirped probe pulse copropagates with the avalanche-driving pulse and passes through the transient plasma into a near-IR spectrometer, while the backscattered driver light is collected by a PbSe photodetector filtered with a germanium window to reject stray visible and near-IR light (see Fig. 1 and Materials and Methods). A probe reference spectrum was also collected for each new set of laser parameters by inserting a borosilicate glass window in the beam path, allowing the probe to be transmitted into the spectrometer but absorbing the λ = 3.9 μm laser light, preventing plasma formation. The probe chirp was measured using cross correlation with a 200-fs, 1030-nm pulse (see Materials and Methods). The probe pulse encodes a wavelength-to-time mapping, enabling the readout of an effective breakdown time by monitoring the reduced probe transmission through the interaction region of the later-in-time wavelength components. We define the breakdown time as corresponding to the wavelength at which the transmitted probe is attenuated by 20% compared with the reference spectrum. Figure 1C shows the transmitted and reference probe spectra and the determination of the breakdown time using their ratio $S_b(\lambda)/S_{ref}(\lambda)$. Probe attenuation can be attributed to a combination of refractive scattering out of the collection solid angle and absorption by the plasma. As the plasma density is well below the critical density

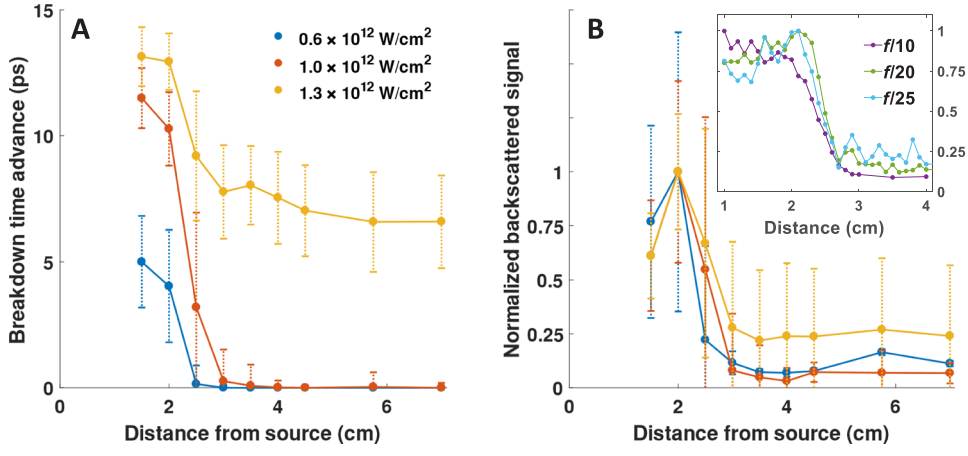

Fig. 2. Breakdown enhancement in the presence of a Po-210 α-particle source. Pulses with peak intensities 0.6, 1.0, and 1.3 × 10^{12} W/cm^2 (pulse energies of 2, 3, and 4 mJ) focused at f/20 drove avalanche breakdowns as the radioactive source was moved 1.5 to 7 cm from the focal spot, with 2500 shots taken at each position. The 5.3-MeV α-particle stopping distance in air is ~3.5 cm (*18*). (**A**) For decreasing radioactive source–focal spot separation, increasing O_2^- seed densities cause faster average avalanche breakdowns, until a maximum breakdown time advance is reached. (**B**) Earlier breakdowns result in increased λ = 3.9 μm pump pulse backscattering by the plasma. Backscatter points are time-integrated signals normalized shot by shot to pulse energy. Each curve is again normalized to its peak signal for comparison between different intensities. The inset of (B) shows backscattering scans for several focal lengths at a fixed peak intensity of 0.7 × 10^{12} W/cm^2, with similar normalization. Error bars indicate the SD of the signal generated from the statistics of 2500 shots at each position and intensity.

N_{cr} of the probe wavelength (at λ = 1.45 μm, $N_{cr} \sim 5 \times 10^{20}$ cm^{-3}), probe scattering is dominant. Our simulations suggest that when the local electron density in the breakdown reaches $N_e \sim 10^{18}$ cm^{-3}, approximately 5% of full single ionization, the region rapidly heats and fully ionizes within a few picoseconds, driving an expanding ionization front that strongly attenuates the pulse. Hence, we take the 20% reduction in probe intensity to correspond to the breakdown having reached a threshold of $N_e \sim 10^{18}$ cm^{-3}.

While the probe reference spectral shape was highly reproducible shot to shot, there were ~4% pulse-to-pulse energy fluctuations. Therefore, for the breakdown time determination, all spectra were first normalized to their peak spectral intensity, which occurred at wavelengths (times) well in advance of observed breakdowns.

Figure 2A shows that as the Po-210 α-source is brought closer to the laser focus, the breakdown time advances by ~5 to 15 ps owing to the increasing density of free electrons and O_2^- ions seeding the avalanche (see later simulations). Here, the avalanche driver pulse is focused at *f*/20. Note that the sharp drop-off near ~2.5 to 3 cm in the curves of Fig. 2A is consistent with a stopping distance of ~3.5 cm in air for 5.3 MeV α-particles (*18*). When the source is sufficiently far from the driver focal volume, lower peak intensities (0.6, 1.0×10^{12} W/cm^2) do not drive the plasma density to saturation (in effect, they do not produce a detectable breakdown), and the probe's spectrum is negligibly attenuated. This produces the zero time-advance points on the plot. Higher peak intensities can drive breakdowns to saturation even in air far enough from the radiation source—here, beyond the α-particle stopping distance—to have a much lower seed density. This is due to the larger volume V_{br} around the focus with an intensity sufficient to drive the breakdown to saturation. Even with the reduced O_2^- densities at longer source-focus distances, it is still likely that there is at least one ion within this volume to seed the avalanche.

The breakdown time advance is reduced because with fewer seed ions present, it is less likely for one to be located near the peak focal intensity. This is seen in Fig. 2A at an intensity of 1.3×10^{12} W/cm^2, where breakdowns with a reduced time advance occur at distances greater than ~4 cm. At this intensity, breakdown occurs even though the O_2^- ion density is markedly lower beyond the stopping distance from the source but still above background because of steady-state diffusion of O_2^- ions from that region. At higher intensity, breakdown can occur even without a radioactive source present, with avalanche seeded by the background ion density of ~10^4 cm^{-3} in ambient air, induced by cosmic rays (*14*, *15*).

In a complementary experiment, we monitored backscattering of the pump light (λ = 3.9 μm) from the avalanching plasma, collected through an *f*/4 imaging lens located at 150° to the incident pump direction (see the PD2 signal in Fig. 1). As seen in Fig. 2B, which plots the normalized scattered light signals, the amount of light collected by the detector markedly increases when the pump focus is close to the radioactive source. For the 1.3×10^{12} W/cm^2 pump, which induces breakdown in unseeded air, a large backscatter signal still occurs at distances from the source beyond the α-particle stopping range. The inset to Fig. 2B shows backscatter results for varying pump focus geometry at a fixed peak intensity of 0.7×10^{12} W/cm^2. The longer *f*/20 and *f*/25 geometries show a backscattering drop-off at longer source-focus distances as well as a larger response at those distances. Longer focal geometries probe larger volumes, enabling sensitivity to lower ion densities. These results illustrate that tuning the avalanche driver pulse energy and focal geometry can optimize the sensitivity of the technique to different seed ion concentrations. As discussed above, the sensitivity limit is set by the naturally occurring cosmic ray–induced O_2^- concentration.

Avalanche on-off sensitivity

As seen in Fig. 2, by appropriately setting the incident laser intensity, there is no detectable breakdown if the source is too far from the laser focus, a nonresponse that would also occur in the absence of a radioactive source.

A clear demonstration of the on-off behavior of avalanche breakdown is shown in Fig. 3, where we record, for breakdowns 1 cm from the source, pump backscatter and breakdown time advance as the α-particle source was blocked and unblocked by a mechanical shutter. Consecutive runs of 100 shots with the shutter open and closed are shown. For 1- to 10-mJ pulses with our backscatter collection geometry and photodetector, the plasma must reach 10^{17} to 10^{18} cm^{-3}, approximately 1 to 10% of full single ionization of air, to be detectable. We note

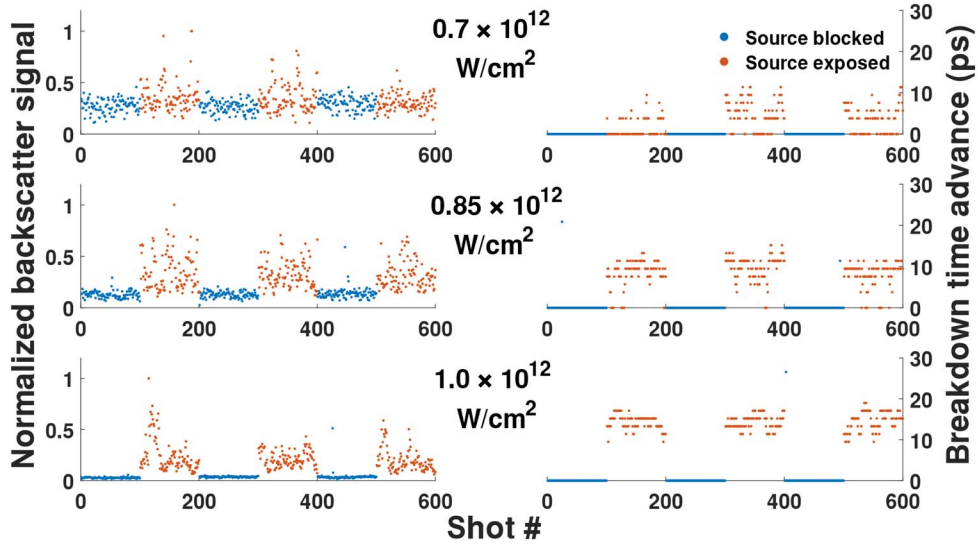

Fig. 3. On-off response of breakdowns to a modulated external source of radioactivity. A series of shots measured the pump backscatter (left) and breakdown time advance (right) as the α irradiation was periodically switched on and off using a mechanical shutter.

that the backscatter signal contrast between "on" and "off" improves substantially with laser intensity. This is due to earlier avalanche breakdown at higher intensities, as seen by the strong increase in the breakdown time advance shown in Fig. 2A. An avalanche occurring earlier in the pulse temporal envelope ensures that more pulse energy is backscattered, improving the contrast. As intensity is further increased, however, breakdowns can occur because of the low density of background ions present in nonirradiated air, degrading the contrast.

In addition, the visible plasma recombination fluorescence exhibits on-off emission as seen in a movie showing the effect of the mechanical shutter blocking and unblocking the line of sight between the Po-210 α-particle foil source and the laser focus (movie S1). Plasma fluorescence emission from the avalanche is therefore an additional radiation-sensitive detection channel. In a related experiment, a separate gas flow O_2^- ion source (from a 0.33 barg airflow past a 20-mCi Po-210 α-particle emitter) was aimed toward and away from the laser focus, with visible fluorescence from air avalanche breakdown occurring only when the source is aimed at the focus (movie S2).

Onset of avalanche: Initial two-photon ionization of O_2^-

As observed in our earlier avalanche experiments using λ = 0.8 μm near-IR pulses at both ~200 ps and ~10 ns (*16*), the minimum peak intensity level required to drive a detectable avalanche also multiphoton ionizes neutral oxygen molecules at the leading edge of the pulse, generating a free-electron density that completely masks the contribution from radioactive sources. Under these conditions, the avalanche was no longer sensitive to the presence of the radioactive source. This is easily understood: At the long-pulse air breakdown threshold of $I_{th} \sim 5 \times 10^{11}$ W/cm^2 for λ = 0.8 μm (*4*, *15*), the rate for MPI (*19*) of neutral oxygen (n = 8 photon process for an ionization potential of 12 eV) is $\nu_{MPI} \sim 2 \times 10^{-4}$ s^{-1}, which predicts an electron density of ~10^6 cm^{-3} in 1 ns, approximately two orders of magnitude higher than the density of background O_2^- ions from cosmic rays (*14*, *15*) and comparable to the density of O_2^- ions induced by the radioactive source in the current experiment. Given that practical implementation of the technique requires operating above the avalanche threshold, the deleterious MPI-generated electron density would further increase. The same trend holds for near-IR picosecond breakdowns, since MPI increases markedly as the intensity is raised to drive a faster breakdown.

In the mid-IR, however, the ionization probability of neutral oxygen drops drastically because of the characteristic I^n scaling of MPI [where n = 38 for λ = 3.9 μm (photon energy, ~0.25 eV)], while two-photon detachment of electrons from O_2^- ions (ionization potential, 0.45 eV) occurs at a much higher probability. The rate of 38-photon MPI (*19*) per neutral oxygen molecule by a λ = 3.9 μm, $I \sim 1 \times 10^{12}$ W/cm^2 pulse is $\nu_{MPI} \sim 3 \times 10^{-21}$ s^{-1}. By comparison, electrons from O_2^- ions are detached by a two-photon process at an enormously higher rate (see below). Although ions generated by radioactive decay include many other species in the reaction chain from the O_2^- precursor (such as NO_2^-, NO_3^-, CO_2^-, O_3^-, O^-, and OH^-), their detachment energies, ranging from 1.5 to 4 eV (*20*), require 5 to 10 photons at λ = 3.9 μm, making their ionization probabilities negligible compared with that from two photon-detachment of O_2^-.

At the onset of avalanche breakdown, the O_2^- ions must first be photodetached before contributing to the electron cascade process. To determine when in the λ = 3.9 μm pulse envelope (FWHM, 50 ps; peak intensity, 0.8×10^{12} W/cm^2) the initial two-photon detachment of O_2^- occurs, we compared the avalanche breakdown time advance with and without single-photon ionization of O_2^- by a copropagating λ = 1.064 μm prepulse (90 ps; peak intensity, 6×10^8 W/cm^2; photon energy, ~1.2 eV), which should ionize ~10% of the initial ion population (see Materials and Methods) (*15*). The prepulse was adjusted to arrive 0.5 or 1 ns before the λ = 3.9 μm pulse. For this experiment, the Po-210 α-particle source was located ~1 cm from the laser focus. Using the chirped λ = 1.45 μm probe pulse, we did not observe any breakdown time advance induced by the λ = 1.064 μm prepulse. This suggests that for these conditions, two-photon ionization of O_2^- takes place very early in the λ = 3.9 μm pulse, over several picoseconds at most. Previous theoretical work gives a two-photon detachment rate per O_2^- ion of $\nu_{2p} \sim 10^{-12}\,[I\,(\mathrm{W/cm^2})]^2$ s^{-1} (*21*). This predicts 10% ionization over $\nu_{2p}^{-1}/10 \sim 2.5$ ps at an early time intensity of 0.2×10^{12} W/cm^2 (one-fourth the peak intensity).

Using $N_{O_2} \sim 5 \times 10^{18}$cm^{-3} and $N_{O_2^-} \sim 10^6$ cm^{-3}, which is in the range of O_2^- ion densities estimated in our experiments (see below), the ratio of electron liberation rates from MPI of neutral O_2 and two-photon ionization of O_2^- is $\nu_{MPI} N_{O_2} / (\nu_{2p} N_{O_2^-}) \sim 10^{-20}$ at $I \sim 1 \times 10^{12}$ W/cm^2. This is negligible, even for considerably higher pump intensities. It is therefore clear that avalanches driven by a λ = 3.9 μm laser pulse are essentially solely seeded by O_2^- ions. Given this scenario, it appears that air avalanches driven by higher laser intensities in the absence of a radioactive source are seeded by the background O_2^- ion concentration of ~10^4 cm^{-3} (*14*, *15*).

Further insight into the role of negative ions in seeding avalanche breakdown was obtained by irradiating a flow of pure nitrogen with the Po-210 α-particle source. In a pure N_2 environment, free electrons produced by ionizing radiation and knock-off electrons do not form negative ions, since N_2^- is an unbound state (*20*). Thus, avalanche breakdown in irradiated nitrogen is seeded by free electrons. When comparing the Po-210–irradiated nitrogen breakdown to one in air (both located 1 cm from the source), there was no detectable shift (>2.5 ps) in the breakdown time advance, from which we infer that the local free electron density in the irradiated nitrogen sample is roughly comparable to the O_2^- density in the air.

Initial ion densities

To more fully characterize the seed ionization level generated by the 5.3-MeV α-particles from the Po-210 source, we compared the breakdowns of air irradiated by this source to breakdowns seeded by a corona discharge ion generator whose ion production is absolutely calibrated with an ion counter (see Materials and Methods). Our results, in Fig. 4, show comparable breakdowns, as measured by breakdown time advance and backscattering, between the two sources when the total negative ion density from the generator is 10^6 to 10^7 cm^{-3}. We note that the background ion density measured by the ion counter far from the radioactive source was ~10^4 cm^{-3}, in agreement with expected negative ion densities in ambient air (*14*, *15*).

Since the ion counter cannot distinguish the types of negative charges collected, this density includes the remainder of the ion reaction chain in addition to the O_2^- ions under study. In addition, some past work suggests that electric discharges and radioactive sources can generate different ratios of ion species (*11*). However, for similar air breakdowns, the counts measured with the ion generator/counter give an order of magnitude estimate of the O_2^- ion density generated by the α source.

A rough estimate of the initial negative ion density can be made given the source activity, the range of α-particles in air, and the average energy needed to create an electron-ion pair (the W-value), from which an ionization rate can be determined. The W-value for a Po-210 α-particle in air is ~35 eV, such that a single decay will produce

~10^5 electron-ion pairs (*22*). Given a CSDA stopping range of ~3.5 cm and the planar source size of 1.7 cm, half of the decay products will be emitted from the foil (2.5 mCi ~ 10^8 decays/s) in a volume of ~150 cm^3. This predicts an ionization rate of ~7 × 10^{10} cm^{-3} s^{-1}, which is ~10^9 times higher than the ionization rates from background radioactivity from cosmic rays and ambient sources such as radon (*14*, *15*). Solving the steady-state rate equations presented in (*15*) with this ionization rate gives an O_2^- ion density of ≥10^8 cm^{-3}. Ion densities are likely lower in practice because of ion diffusion, air convection, and energy lost by the α-particle as it leaves the foil source.

Modeling and simulation

Results of a simple numerical model of ionization adapted from (*15*) are shown for a range of laser intensities and initial O_2^- densities in Fig. 5. In Fig. 5A, plasma evolution seeded by a single electron versus the local peak intensity is calculated for a Gaussian pulse with τ_{FWHM} = 50 ps centered at t = 0 ps and terminated at t = ± 35 ps, consistent with cross-correlation measurements of our pump beam. Breakdown time advance is defined as the time difference between the plasma density reaching 10^{18} cm^{-3}, when the simulation predicts a rapid increase in plasma density toward saturation, and the end of the pulse at t = 35 ps. The simulation results are broadly consistent with experimental measurements, indicating a breakdown threshold near ~10^{12} W/cm^2. Figure 5B shows a simulation of the statistical spread of time advance for our experimental geometry, based on the probability of finding a seed electron at different locations in the focal volume.

At high seed densities, there is a high probability of an electron occupying the region of peak intensity, such that the mean time advance saturates to the values plotted in Fig. 5A for intensities ≳ 10^{12} W/cm^2. The values of time advance agree roughly with those observed in the experiment but are somewhat larger, likely because of the limited modeling of diffusion losses (see Materials and Methods). Comparing the plot with the time advances in Fig. 2A, we predict O_2^- seed densities ~10^7 cm^{-3} near the α source and between ~10^6 and ~10^5 cm^{-3} beyond the α stopping distance, in line with our previous estimates and measurements in Fig. 4.

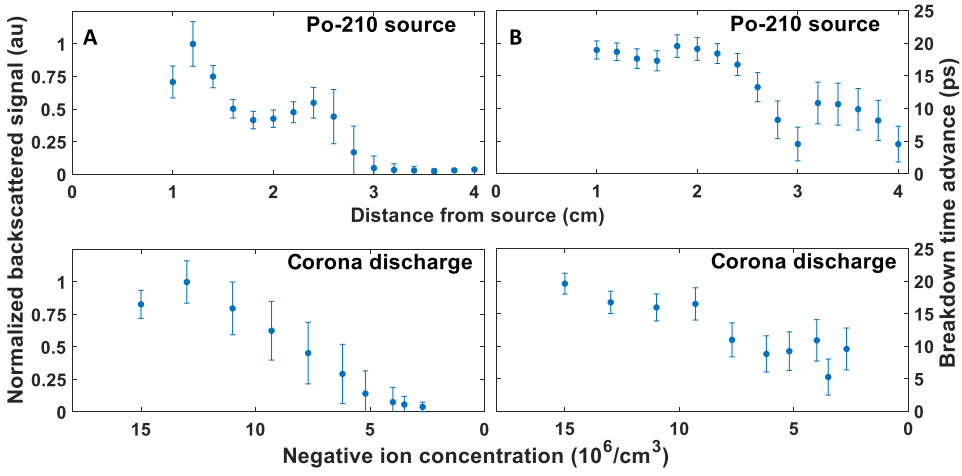

Fig. 4. Comparison of avalanche breakdowns seeded by the Po-210 source and corona discharge ion generator. (**A**) Normalized backscatter signal versus source distance from breakdown seeded by the Po-210 source (top) and versus negative ion concentration from an ion generator (bottom). All shots are for an intensity of ~2 × 10^{12} W/cm^2, which was high enough to ensure breakdowns at every position/ion concentration. (**B**) Breakdown time advance versus distance from breakdown seeded by the Po-210 source (top) and versus negative ion concentration from an ion generator (bottom). Error bars show the SD over 2500 laser shots.

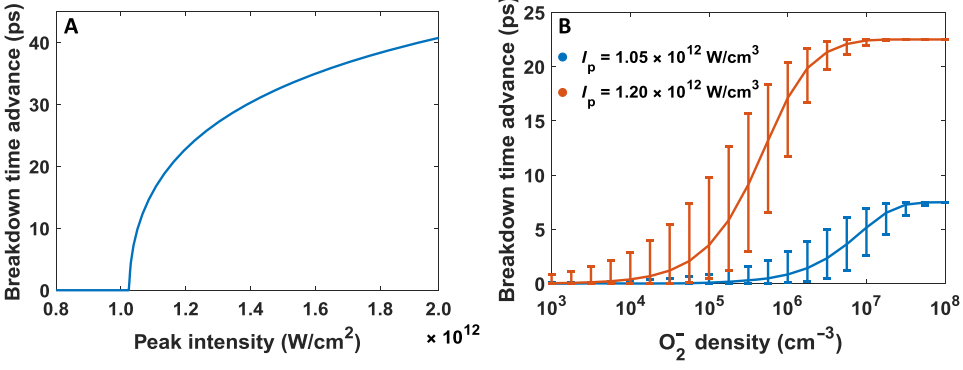

Fig. 5. Simulation of avalanche breakdown. (**A**) Simulation of the breakdown time advance starting from a single electron driven at a range of peak intensities (Gaussian pulse with τ_{FWHM} = 50 ps, terminated at t = ± 35 ps). (**B**) Simulation of the distribution of mean breakdown time advances for different seed O_2^- densities driven by a laser pulse with a peak intensity of 1.05 or 1.2 × 10^{12} W/cm^2 focused at *f*/20, matching experimental conditions. Error bars show the SD of the probability distribution, calculated separately for values above and below the mean. Probability of breakdown times for a given density was calculated using Poisson statistics to determine the probability of an electron occupying volume elements of differing peak intensities throughout the focal volume (see Materials and Methods).

DISCUSSION

Consideration of the avalanche scheme for practical detection situations necessitates scaling to much longer focal geometries and larger spot sizes, with a goal being standoff distances up to ~100 m. Our observed breakdown threshold range of ~0.6 to 0.7 × 10^{12} W/cm^2 provides an estimate of the minimum energy needed to achieve breakdown for different focusing geometries. For example, at *f*/100 (using a 1-m-diameter beam focused at a distance of 100 m), a total energy of ~31 mJ would be required to barely exceed the breakdown threshold at peak intensity for ideal Gaussian beam focusing. By slightly increasing the peak intensity to ~0.8 × 10^{12} W/cm^2, the total volume for which the intensity exceeds the threshold range varies from about 3 × 10^{-5} to 3 × 10^{-4} cm^3, providing sensitivity to seed ion densities of ~10^5 cm^3. For best sensitivity, the laser conditions should be chosen such that the background O_2^- ion density in air from cosmic rays [~10^4 cm^{-3} (*14*, *15*)] is unlikely to seed breakdowns, minimizing the "noise" of this detection scheme. Considerations for detection sensitivity at range are the subject of ongoing work.

For nanosecond pulse–driven breakdown, the threshold intensity is lower owing to the reduced electron density growth rate required to achieve full breakdown over the longer pulse duration, where I_{th} [W/cm^2] ~ 3 × 10^{11}/(λ[μm])^2 (*4*, *23*) in the limit of long pulse widths. Thus, at *f*/100, a ~10-ns square pulse at either λ = 3.9 or 10.6 μm would require ~400 mJ of pump energy. The motivation for considering pulses in the ~10-ns range is that currently available CO_2 transverse excitation atmospheric lasers at λ = 10.6 μm can provide the relevant pulse energies at those pulse durations. While these lasers do not have a smoothly chirped probe beam available as used in the present experiment, they would still achieve proper on-off sensitivity by avoiding the MPI driven by near-IR laser pulses. They are also far more feasible than terahertz sources in availability and focusability.

Although we have used an α-particle source to test our avalanche scheme, our use of an ion generator producing known concentrations allowed us to estimate the ion densities seeding the mid-IR laser–driven avalanche, and these are in reasonable agreement with simulations. Therefore, we can extend our current work to γ sources by considering the source activity and distance to the avalanche location that will give a similar concentration of O_2^- ions. Simulations suggest (*14*, *15*, *24*) that the levels of O_2^- to which we are sensitive in the current experiment (≳10^6 cm^{-3} from Fig. 5) would be present ≲10 m from an unshielded 1-mg (~1 Ci) source of cobalt-60, while lower initial ion densities (5 × 10^4 to 5 × 10^5) would be expected tens of meters from the same source, or ≲1 m from a 1-μg (~1 mCi) cobalt-60 source.

The present experiment used a chirped probe copropagating with the pump to obtain breakdown time advance information, though practical standoff detection will require a backscattered signal. However, as demonstrated above, the backscattered pump signal increased markedly as the breakdown occurred earlier in time. For an appropriate choice of pump intensity (energy), backscattering displayed on/off sensitivity to the presence/absence of an external radiation source. A chirped pump pulse, with backscatter monitored with a mid-IR spectrometer, would enable measurements of breakdown time advance at range, further improving detection sensitivity.

MATERIALS AND METHODS

Laser system and electron avalanche

A schematic of the experimental setup is shown in Fig. 1. Upstream of BS1 in the figure, pump pulses (FWHM, 50 ps; full width, 70 ps; λ = 3.6 to 4.2 μm; ≤20 mJ) and probe pulses [full width, 70 ps; λ = 1.4 to 1.5 μm (nominally 1.45 μJ); ~10 μJ] are both produced in a hybrid OPA (optical parametric amplifier)/OPCPA ultrafast laser system (*25*). Near-IR (λ = 1.4 to 1.5 μm) pulses (the signal) are generated in a three-stage femtosecond OPA pumped by a 1.030-μm pump beam before being dispersed in a grism pulse stretcher to a pulse length of 70 ps. The negatively chirped near-IR signal pulse is then parametrically amplified in an OPCPA by a 1.064-μm pump beam, generating the positively chirped, 50-ps FWHM, λ = 3.6 to 4.2 μm (nominally 3.9 μm) idler pulse used to drive the avalanche. This pulse has been routed to bypass the pulse compressor normally used to produce 90-fs pulses. After the OPCPA, a dichroic beamsplitter BS1 routes the chirped 1.45-μm beam to a photodiode to track shot-to-shot energy fluctuations, and a small amount of leakage (~10 μJ) copropagates with the λ = 3.9 μm pulse for use as a wavelength-to-time encoded probe beam. [Single-shot measurement of transient events using chirped pulses has been used in systems as disparate as optical rogue waves (*26*) and superluminal pulse propagation (*27*).] Air breakdowns were observed in ambient air, seeded by a 5-mCi Po-210 spot foil source from NRD, LLC, or by a negative ion generator (Murata MHM305 corona discharge). An additional source of O_2^- ions used only for movie S2 was a 0.33 barg airflow swept past a 20-mCi Po-210 α-particle source.

Diagnostics

Plasma evolution was probed both by the transmission of a chirped copropagating probe beam (70 ps, 1400 to 1500 nm) gathered with an *f*/2 lens into an Avantes near-IR InGaAs spectrometer, and backscatter of the pump beam incident on a PbSe photodetector filtered with a germanium window to prevent collection of near-IR scattered light. The chirp of the probe beam was measured by cross correlation with a synchronous 200-fs, λ = 1030 nm pump beam, providing the time delay corresponding to each spectral component.

A reference spectrum was taken by placing a borosilicate window in the beam path, absorbing the λ = 3.9 μm pulse, while transmitting the λ = 1.4 to 1.5 μm probe, thus preventing the formation of any air plasma. To account for reflection loss in the window and pulse-to-pulse energy fluctuations, each spectrum was normalized to its peak spectral intensity, which corresponded to a time well before the pulse was attenuated. The threshold for the probe being attenuated was set at 80% of the reference spectrum's intensity.

Calibration of the negative ion generator was performed with an AlphaLab Gerdien condenser meter. Because of the large gradient in ion density near the α source compared with the size of the condenser meter air intake, it was not feasible to perform measurements of the α source with the condenser meter, but comparison of breakdowns seeded by the ion generator and the α source (Fig. 4) allowed rough estimates of the initial seed density for the radioactive source.

Modeling and simulation

Evolution of the electron avalanche in the laser field was modeled using coupled rate equations for electrons, neutrals, positive ions, and negative ions (dominated by O_2^- on the experimental time scale) as detailed in (*15*). The rate equations include single-photon ionization and MPI, collisional ionization, electron attachment, electron-ion dissociative recombination, and collisional negative ion detachment as a function of the plasma temperature, density, and laser pulse intensity. However, since the current experiment operates in a different regime from that presented in (*15*), we have adjusted the model to account for statistical breakdown and higher equilibrium temperatures. In the picosecond

breakdown regime, a higher temperature (and collisional rate) is required to achieve ionization saturation before the end of the pulse. At these higher temperatures, energy loss due to molecular dissociation and ionization markedly increases, so we included numerical values for these loss rates presented in (*23*, *27*). In addition, for much of the seed density range of our experiment, avalanches are locally seeded in the laser focus by single or multiple isolated ions and not by a locally continuous density as in (*15*). Hence, what is needed for proper simulation of avalanches proceeding from single charges is the electron density growth rate and plasma temperature T_e for a given air density and peak laser intensity, which were extracted for a range of intensity values at atmospheric density. These rates were then used to evolve a breakdown beginning with a single seed electron experiencing a Gaussian intensity pulse, and densities were calculated using an effective volume $\frac{4}{3}\pi r_{\mathrm{diff}}^3$ derived from electron diffusion. Here, $r_{\mathrm{diff}} \sim (2D_e/\nu)^{1/2}$, where $D_e = k_B T_e/m_e\nu$ is the diffusion coefficient, k_B is the Boltzmann's constant, m_e is the electron mass, and ν is the electron collision frequency with neutrals and ions. Although this approach gives reasonable agreement for the intensity threshold for achieving breakdown, at higher driving intensities and plasma temperatures, additional diffusion driven by thermal and pressure gradients would likely reduce the inferred time advance.

To generate a distribution of breakdown times, Poisson statistics were used to calculate the probability of finding an electron at various locations in the focal volume of a *f*/20, ~100-μm FWHM focal spot. The probability that a given intensity I will determine the breakdown time advance is given by PP', where $P = 1 - e^{-\lambda}$ is the probability that at least one electron occupies the volume corresponding to that intensity and $P' = e^{-\lambda'}$ is the probability that no electron occupies the volume of higher intensity, where $\lambda = NV$ is the average number of electrons in the volume of interest.

To estimate the initial equilibrium ratio of electron density to O_2^- density, we consider only the rate equation for O_2^- ions, $\frac{\partial N_{O_2^-}}{\partial t} = -\nu_{2p}(I)N_{O_2^-} + \eta N_e N_{O_2}^2 - \beta_n N_n N_{O_2^-}$, where $\nu_{2p}(I)N_{O_2^-}$ is the intensity-dependent rate ($cm^{-3}\,s^{-1}$) of two-photon ionization ($\nu_{2p} = 0$ before the pulse arrives), $\eta N_e N_{O_2}^2$ is the three-body attachment rate of electrons to neutral O_2, and $\beta_n N_n N_{O_2^-}$ is the detachment rate from collisions of O_2^- ions with neutrals (density N_n), and we assume $N_n/N_{O_2} = 5$. The rate coefficients η and β_n are found in (*15*). As discussed, the initial electron, O_2^-, and positive ion densities are small compared to the neutral gas density, so we have neglected terms in (*15*) that correspond to electron-ion interactions.

SUPPLEMENTARY MATERIALS

Supplementary material for this article is available at http://advances.sciencemag.org/cgi/content/full/5/3/eaav6804/DC1

Movie S1. ON-OFF response of laser-induced avalanche to external radioactive source.

Movie S2. ON-OFF response of laser-induced avalanche to radioactivity-induced oxygen ions from an airflow source.

REFERENCES AND NOTES

1. A. D. MacDonald, *Microwave Breakdown in Gases* (Wiley,1966).
2. Y. P. Raizer, Breakdown and heating of gases under the influence of a laser beam. *Sov. Phys. Usp.* **87**, 29–64 (1965).
3. C. G. Morgan, Laser-induced breakdown of gases. *Rep. Prog. Phys.* **38**, 621–665 (1975).
4. N. Kroll, K. M. Watson, Theoretical study of ionization of air by intense laser pulses. *Phys. Rev. A* **5**, 1883–1905 (1972).
5. C. G. Durfee III, J. Lynch, H. M. Milchberg, Development of a plasma waveguide for high-intensity laser pulses. *Phys. Rev. E* **51**, 2368–2389 (1995).
6. V. L. Granatstein, G. S. Nusinovich, Detecting excess ionizing radiation by electromagnetic breakdown of air. *J. Appl. Phys.* **108**, 063304 (2010).
7. G. S. Nusinovich, P. Sprangle, C. A. Romero-Talamas, V. L. Granatstein, Range, resolution and power of THz systems for remote detection of concealed radioactive materials. *J. Appl. Phys.* **109**, 083303 (2011).
8. D. Kim, D. Yu, A. Sawant, M. S. Choe, I. Lee, S. G. Kim, E. Choi, Remote detection of radioactive material using high-power pulsed electromagnetic radiation. *Nat. Commun.* **8**, 15394 (2017).
9. M. L. Huertas, J. Fontan, J. Gonzalez, Evolution times of tropospheric negative ions. *Atmos. Environ.* **12**, 2351–2362 (1967).
10. V. A. Mohnen, Discussion of the formation of major positive and negative ions up to the 50 km level. *Pure Appl. Geophys.* **84**, 141–151 (1971).
11. M. L. Huertas, J. Fontan, Formation of stable positive and negative small ions of tropospheric interest. *Atmos. Environ.* **16**, 2521–2527 (1982).
12. A. A. Viggiano, F. Arnold, Ion chemistry and composition of the atmosphere, in *Handbook of Atmospheric Electrodynamics*, H. Volland, Ed. (CRC Press, 1995), vol. 1.
13. K. M. Ervin, I. Anusiewicz, P. Skurski, J. Simons, W. C. Lineberger, The only stable state of O_2^- is the X $^2\Pi_g$ ground state and it (still!) has an adiabatic electron detachment energy of 0.45 eV. *J. Phys. Chem. A* **107**, 8521–8529 (2003).
14. P. Sprangle, B. Hafizi, H. M. Milchberg, G. S. Nusinovich, A. Zigler, Active remote detection of radioactivity based on electromagnetic signatures. *Phys. Plasmas* **21**, 013103 (2014).
15. J. Isaacs, C. Miao, P. Sprangle, Remote monostatic detection of radioactive material by laser-induced breakdown. *Phys. Plasmas* **23**, 033507 (2016).
16. D. Woodbury, J. Wahlstrand, A. Goers, L. Feder, B. Miao,G. Hine, F. Salehi, H. Milchberg, Single-shot measurements of laser-induced avalanche breakdown demonstrating spatial and temporal control by an external source, Presentation CP10.00154, American Physical Society Division of Plasma Physics Meeting, Oct. 2016.
17. J. Way, J. Hummelt, J. Scharer, Experimental measurements of multiphoton enhanced air breakdown by a subthreshold intensity excimer laser. *J. Appl. Phys.* **106**, 083303 (2009).
18. National Institute of Standards and Technology; http://physics.nist.gov/PhysRefData/Star/Text/ASTAR.html.
19. A. M. Perelomov, V. S. Popov, M. V. Terent'ev, Ionization of atoms in an alternating electric field. *Sov. Phys. JETP* **23**, 924–934 (1966).
20. J. C. Rienstra-Kiracofe, G. S. Tschumper, H. F. Schaefer, S. Nandi, G. B. Ellison, Atomic and molecular electron affinities: Photoelectron experiments and theoretical calculations. *Chem. Rev.* **102**, 231–282 (2002).
21. N. M. Kroll, K. M. Watson, Multiphoton detachment of negative ions, DARPA Final Technical Report JSR-73-6 (1974).
22. W. P. Jesse, J. Sadauskis, Ionization in pure gases and the average energy to make an ion pair for alpha and beta particles. *Phys. Rev.* **97**, 1668–1670 (1955).
23. A. W. Ali, Electron energy loss rates in N_2, O_2, and air, NRL Memorandum Report 5400 (1984).
24. Y. S. Dimant, G. S. Nusinovich, P. Sprangle, J. Penano, C. A. Romero-Talamas, V. L. Granatstein, Propagation of gamma rays and production of free electrons in air. *J. Appl. Phys.* **112**, 083303 (2012).
25. G. Andriukaitis, T. Balčiūnas, S. Ališauskas, A. Pugžlys, A. Baltuška, T. Popmintchev, M. C. Chen, M. M. Murnane, H. C. Kapteyn, 90 GW peak power few-cycle mid-infrared pulses from an optical parametric amplifier. *Opt. Lett.* **36**, 2755–2757 (2011).
26. D. R. Solli, C. Ropers, P. Koonath, B. Jalali, Optical rogue waves. *Nature* **450**, 1054–1057 (2007).
27. I. Alexeev, K. Y. Kim, H. M. Milchberg, Measurement of the superluminal group velocity of an ultrashort Bessel beam pulse. *Phys. Rev. Lett.* **88**, 073901 (2002).

Acknowledgments: We thank J. K. Wahlstrand for assistance with the calculation of MPI rates. **Funding:** This research was supported by the Defense Threat Reduction Agency (HDTRA11510002), Air Force Office of Scientific Research (FA9550-16-10121 and FA9550-16-10259), and the Office of Naval Research (N00014-17-1-2705). D.W. acknowledges support from the DOE NNSA SSGF program (DE-NA0003864). **Author contributions:** H.M.M. and P.S. conceived the detection method. H.M.M., R.M.S., and D.W. conceived the experiment. R.M.S. and D.W. carried out the experiment and performed the data analysis. D.W., J.I., and P.S. developed the simulation model. D.W. performed the simulations. D.W., R.M.S., and H.M.M. prepared the manuscript, with input from all authors. **Competing interests:** The authors declare that they have no competing interests. **Data and materials availability:** All data needed to evaluate the conclusions in the paper are present in the paper and/or the Supplementary Materials. Additional data related to this paper may be requested from the authors.

Submitted 10 October 2018
Accepted 31 January 2019
Published 22 March 2019
10.1126/sciadv.aav6804

Citation: R. M. Schwartz, D. Woodbury, J. Isaacs, P. Sprangle, H. M. Milchberg, Remote detection of radioactive material using mid-IR laser–driven electron avalanche. *Sci. Adv.* **5**, eaav6804 (2019).

Science Advances

Remote detection of radioactive material using mid-IR laser–driven electron avalanche

Robert M. Schwartz, Daniel Woodbury, Joshua Isaacs, Phillip Sprangle and Howard M. Milchberg

Sci Adv **5** (3), eaav6804.
DOI: 10.1126/sciadv.aav6804